

# Direct Forcing for Lagrangian Rigid-Fluid Coupling

Markus Becker, Hendrik Tessendorf, Matthias Teschner

**Abstract**—We propose a novel boundary handling algorithm for particle-based fluids. Based on a predictor-corrector scheme for both velocity and position, one- and two-way coupling with rigid bodies can be realized. The proposed algorithm offers significant improvements over existing penalty-based approaches. Different slip conditions can be realized and non-penetration is enforced. Direct forcing is employed to meet the desired boundary conditions and to ensure valid states after each simulation step. We have performed various experiments in 2D and 3D. They illustrate one- and two-way coupling of rigid bodies and fluids, the effects of hydrostatic and dynamic forces on a rigid body as well as different slip conditions. Numerical experiments and performance measurements are provided.

**Index Terms**—Physically-based simulation, Fluid dynamics, Smoothed Particle Hydrodynamics, Rigid bodies, Boundary handling

## I. INTRODUCTION

THE simulation of fluids has attracted increasing attention in Computer Graphics in recent years. Various sophisticated methods have been proposed and a thorough introduction of fluid simulation techniques has been presented by Bridson and Müller-Fischer in their ACM SIGGRAPH'07 course notes [1].

As a fluid is generally simulated in a domain with fixed and moving obstacles, it is necessary to consider the interaction of the fluid with these obstacles. Often, different kinds of boundary conditions need to be incorporated. While this problem has been dealt with extensively in the context of grid-based methods, there are still only a few approaches to boundary conditions for particle-based methods such as Smoothed Particle Hydrodynamics (SPH). This is to some extent due to the fact that one is interested in preserving the local nature given in many Lagrangian fluid simulations. Despite these challenges, the interest in boundary conditions for particle-based fluids is motivated by the usefulness of Lagrangian fluids for irregular domains. Typically applied penalty methods as e. g. provided by Monaghan [2] offer only limited control of the boundary handling. To enforce non-penetration, large penalty forces have to be applied which introduce stiffness to the equations.

We propose a novel method for the two-way coupling of compressible Lagrangian fluids and rigid objects. Control forces are incorporated in the discretized momentum equations in order to obtain specific relative velocities at a boundary in each timestep. This is known as direct forcing. It is realized in a predictor-corrector fashion. Using the proposed formulation, a large range of slip and Neumann boundary conditions can be imposed for arbitrarily shaped, fixed or moving boundaries. Regularly and irregularly shaped boundaries can be handled in a unified manner. Dynamic and hydrostatic fluid forces acting on the boundaries are considered. The local nature of employed SPH method is

preserved by the boundary handling. Many drawbacks of penalty-based methods such as oscillations at the boundary and limited control of the boundary conditions can be avoided.

The proposed technique extends previous Lagrangian boundary approaches such as the one of Hieber [3]. In contrast to [3], it avoids force interpolations and it guarantees non-penetration for fixed and moving rigid boundaries. To enforce the boundary velocities, we adopt the interpenetration resolution proposed in [4], [5]. Fluid leaking through boundaries is avoided by controlling particle velocities and positions in separate substeps. A minimal parameter set with a known parameter range allows for an intuitive setup of the simulation.

Experiments are performed using the corrected SPH algorithm of Bonet and Kulasegaram [6] and the weakly compressible pressure formulation described e. g. in [7] and [8]. Fig. 1 illustrates a first example. In this stone-skipping simulation, the reflection of the stone from the fluid surface is realized using the proposed boundary handling.

The remainder of the paper is organized as follows. After discussing related approaches in Sec. II, we briefly describe the employed fluid model and the particle-based representation of the rigid bodies in Sec. III and Sec. IV, respectively. The boundary handling approach for the two-way coupling of Lagrangian fluids and rigid objects is presented in Sec. V. Parameters, implementation issues and limitations are discussed. In Sec. VI, various experiments are described to illustrate the capabilities of the proposed approach. The experiments cover the major features of the boundary handling approach. They include a comparison with the penalty approach of [2], performance measurements, the effects of hydrostatic and dynamic forces, as well as one- and two-way coupling.

## II. RELATED WORK

In this section, we discuss some related literature concerning boundary handling and rigid-fluid coupling for different fluid simulations. The related work covers Eulerian boundary handling approaches, mixed formulations and Lagrangian approaches.

Many sophisticated solutions have been proposed for the solid-fluid coupling of Eulerian fluids and early coupling approaches date back to e. g. Chen and Lobo [9]. The authors introduce two types of one-way coupling for a 2D Navier-Stokes solver where the third dimension is modeled using a height field. An idea for the two-way coupling is outlined, but not implemented. Various authors have realized a one-way solid-fluid coupling and fixed boundaries in 3D by voxelizing the boundaries on the fluid grid [10]–[13]. These approaches commonly adjust the fluid velocity of grid points covered by the solid to the velocity of the solid. Several improvements have been proposed, e. g. a corrected normal for free tangential slip [14]. Still, this method tends to produce stair-step artifacts for boundaries that are not aligned with the grid. This is especially noticeable in the case of coarse grids. Takahashi et al. [15] provide a simple two-way coupling



Fig. 1. Three frames of a stone-skipping simulation. The stone is reflected from the surface in case of an impact. This effect is obtained using a novel two-way coupling approach of rigid bodies and particle-based fluids.

for voxelized buoyant rigid bodies. They take the pressure on the surface into account. However, dynamic forces, i. e. forces due to relative velocities in the fluid, are neglected. Yngve et al. [16] provide an approach to the two-way coupling of deformable and fracturing solids with a compressible fluid. Still, solids need to be voxelized on the grid in order to realize a solid-to-fluid coupling.

To avoid voxelization artifacts, some authors have proposed to adaptively align the fluid grid at boundaries or to use remeshing. An octree refinement is introduced by Losasso et al. [17]. Irving et al. [18] introduce a regular one-layer refinement for MAC grids with moving objects. Klingner et al. [19] and Chentanez et al. [20] address irregular geometries by using tetrahedral meshes for the fluid simulation. The mesh is regenerated in each timestep according to the current configuration of the boundaries. [19] is extended by Chentanez et al. [21] to handle both rigid and deformable solids. Feldman et al. [22] handle moving boundary conditions by deforming the underlying simulation mesh.

There exist alternative concepts to incorporate boundary conditions for Eulerian fluids. Batty et al. [23] improve the FLIP method of [24] for two-way rigid-fluid coupling. In this approach, the pressure projection is formulated as a kinetic energy minimization problem. Carlson et al. [25] use Distributed Lagrangian multipliers to project fluid nodes covered by rigid bodies onto rigid body motion. Genevaux et al. [26] use damped springs to attach solids to fluid marker particles. Guendelmann et al. [27] present an alternating two-way coupling for deformable and rigid thin shells. This algorithm uses ray-casting to avoid fluid leaking through thin solids represented by triangles. Liu et al. [28] present a GPU approach for the semi-Lagrangian scheme of Stam [12]. Arbitrary boundary conditions for the fluid simulation are generated directly in image space.

Some authors propose a mixed formulation, using an Eulerian formulation for the fluid and a Lagrangian formulation for the solid. The Immersed Boundary Method (IBM) introduced by Peskin [29], [30] samples a solid with a finite set of force points. As the boundary velocities are interpolated on the grid, boundaries are not required to coincide with the fluid grid. Therefore, the approach is appropriate for irregular and detailed geometries. In the context of IBM, direct forcing has been employed [31]–[33]. A force term is added to the discretized momentum equations to obtain the adequate velocity of the fluid along the boundary after a single timestep. This direct forcing approach is free of parameters and can therefore be handled conveniently. The Immersed Interface Method of Le et al. [34] improved on IBM for rigid boundaries and moving deformable solids. It can handle sharp interfaces, since forces are not distributed on the boundary.

Fedkiw [35] uses so-called ghost fluid nodes to couple compressible Eulerian fluids and deformable Lagrangian solids. Ghost fluid nodes can be covered by the solid, but are used in the finite difference scheme for the fluid update. The Eulerian and the Lagrangian parts of the simulation are properly interpolated. Combining Eulerian grids and Lagrangian meshes has also been proposed in the finite-element ALE (Arbitrary Lagrangian Eulerian) method of Hirt et al. [36]. A mixed formulation that couples SPH particles and particle level sets has been introduced by Losasso et al. [37] to reduce volume loss for free surfaces. Robinson-Mosher et al. [38] recently proposed an approach to couple Cartesian fluid grids and Lagrangian solids derived from the law of conservation of momentum.

Most of the aforementioned methods cannot directly be applied to pure particle-based fluids and only a few methods have been proposed for pure particle-based simulations until now. Most authors use penalty-based approaches to handle static or moving rigid boundaries. The main concept of penalty-based approaches is to use either frozen or ghost particles. Frozen particles interact with other particles in the usual way, but they do not move. Ghost particles on the other hand are fluid particles mirrored across solid boundaries in each timestep. Monaghan [2] proposes a force-based penalty method for fixed and moving boundaries and in [6], a penalty boundary potential is used to calculate penalty forces. Keiser et al. [39] present a Lagrangian formulation to handle solids, fluids, and phase transitions. Solenthaler et al. [40] and Keiser et al. [41] process fluid and rigid-body particles in similar ways. Rigid-body particles are restricted to rigid-body motion in the update step. Falappi and Galatti [42] handle interacting fluids and granular materials by using SPH for both phases. Müller et al. [43] employ a penalty approach based on Lennard-Jones forces for repulsion and adhesion between mesh-based deformable solids and particle-based fluids.

There have been few approaches that try to model different kinds of boundary conditions with penalty methods. Ghost particles with the same mass, density, pressure and viscosity, but different velocity than their fluid counterpart have been employed to handle different slip conditions for straight [44] and curved [45] surfaces. However, penalty methods suffer from severe difficulties. As penalty forces only react upon penetration, the distance of SPH particles to the boundary slightly varies over time and particles might be accelerated at the boundary. Only limited control is offered to realize specific boundary conditions. Most approaches so far do not offer an easy way to adjust tangential damping in the full range from no- to free-slip. Finally, to ensure non-penetration, large forces have to act on the fluid,

leading to stiff equations. To illustrate the benefits of the proposed direct forcing approach, we provide a comparison with the penalty approach of [2] in Sec. VI.

Few approaches have taken into account the actual forces acting on the boundary for the boundary handling so far. Oger et al. [46] propose a method for the two-way coupling of a particle-based fluid and a moving solid in two dimensions. However, only the local pressure on the solid surface is evaluated. Dynamic forces, e. g. due to viscosity, are neglected. Hieber [3] adopts IBM for the boundary handling of particle-based fluids with deformable solids and fixed boundaries, thereby allowing a greater amount of control of the fluid and taking into account all forces acting on the boundary. However, non-penetration is not addressed. Additionally, a fixed number of Lagrangian force points is used to sample the boundary and an underlying Eulerian grid is used to transfer values between the fluid simulation and the force points. We share the idea of [3] to modify the underlying momentum equation to ensure the chosen boundary conditions with a direct forcing approach. However, in contrast to [3], forces can be applied directly at the contact point and thereby, force interpolations are avoided. Non-penetration is guaranteed after each timestep and fluid leaking is avoided. This is especially important for the two-way coupling with rigid bodies due to the limited number of degrees of freedom. We furthermore propose a simple scheme to cover different kinds of velocity boundary conditions. The approach is realized in a predictor-corrector fashion.

The concept of direct forcing has been successfully applied in other simulation areas such as constraint handling for rigid [47]–[49] and deformable [50], [51] solids. However, these approaches are beyond the scope of this paper. The same applies to boundary conditions for other fluid methods such as the Lattice Boltzmann method [52]. The idea of predictor-corrector schemes has also been successfully applied in contact and collision handling for rigid and deformable bodies, see e. g. [4], [53].

### III. FLUID MODEL

For the fluid simulation, we use a corrected SPH formulation (CSPH) [6] and the weakly compressible pressure formulation employing the Tait equation [7], [8].

The basic idea of SPH is to represent a function  $f(\mathbf{x})$  as a smoothed function  $\langle f(\mathbf{x}) \rangle$  using a finite set of sampling points  $\mathbf{x}_b$  with mass  $m_b$  and density  $\rho_b$ , and a kernel function  $W_b(\mathbf{x}) = W(\mathbf{x} - \mathbf{x}_b)$ :

$$\langle f(\mathbf{x}) \rangle = \sum_b \frac{m_b}{\rho_b} f(\mathbf{x}_b) W_b(\mathbf{x}). \quad (1)$$

However, this original SPH formulation developed independently by Gingold and Monaghan [54] and Lucy [55] suffers from inaccurate calculations at boundaries. Since the number of neighboring particles at boundaries is smaller than inside the fluid, an incorrect lower density is calculated and negative pressures can occur. As we extensively deal with boundaries in rigid-fluid coupling, we address this problem by using the constant correction technique for SPH proposed in [6]. By using an adapted kernel function

$$\tilde{W}_b(\mathbf{x}) = \frac{W_b(\mathbf{x})}{\sum_c V_c W_c(\mathbf{x})} \quad (2)$$

for the density calculation, this model avoids inaccurate pressures at boundaries. The overhead for the computation of the adapted kernel function  $\tilde{W}_b(\mathbf{x})$  is negligible. Since the volume  $V_c$  of a particle is constant, it can be precomputed. Thus, an additional

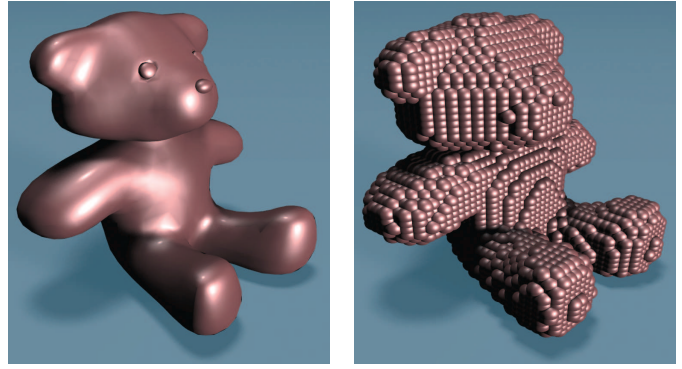


Fig. 2. Triangulated surface and particle representation of the teddy model.

loop over the particles is avoided. For the computation of the fluid dynamics, we use the reformulated Euler equation with external forces denoted by  $\mathbf{g}$

$$\frac{d\mathbf{v}}{dt} = - \left( \nabla \left( \frac{P}{\rho} \right) + \frac{P}{\rho^2} \nabla \rho \right) + \mathbf{g} \quad (3)$$

with pressure  $P$ , density  $\rho$  and velocity  $\mathbf{v}$ . It results in a symmetrized discrete momentum equation that conserves linear and angular momentum [2]. The discrete momentum equation for the acceleration  $\frac{d\mathbf{v}_a}{dt}$  of a particle with added artificial viscosity [2] and the original kernel function  $W_b$  thereby reads

$$\frac{d\mathbf{v}_a}{dt} = - \sum_b m_b \left( \frac{P_a}{\rho_a^2} + \frac{P_b}{\rho_b^2} + \Pi_{ab} \right) \nabla_a W_b(\mathbf{x}_a) + \mathbf{g} \quad (4)$$

with the viscosity term

$$\Pi_{ab} = -\nu \left( \frac{\mathbf{v}_{ab}^T \mathbf{x}_{ab}}{|\mathbf{x}_{ab}|^2 + \delta h^2} \right). \quad (5)$$

The pressure  $P$  is calculated using the Tait equation [7], [8] to ensure small density ratios between the current density  $\rho$  and the initial density  $\rho_0$

$$P = \frac{\rho_0 c_s^2}{7} \left( \left( \frac{\rho}{\rho_0} \right)^7 - 1 \right). \quad (6)$$

The speed of sound  $c_s$  is usually chosen such that the Mach number of the simulation is below 0.1. For further details see e. g. [8].

### IV. RIGID BODY MODEL

In the context of rigid-fluid coupling, various rigid-body representations have been proposed, e. g. triangle meshes [43], adaptively sampled distance fields [56], and particles [2]. Similar to [2], we employ a particle representation for arbitrary rigid-body surfaces. The particle representation is generated in a preprocessing step using a distance field [57]. An example is shown in Fig. 2.

Although the proposed rigid-body representation allows for a unified handling of rigid bodies and fluids in certain aspects of the simulation, e. g. particle-particle collision tests, our boundary handling approach could be combined with alternative representations such as triangle meshes or distance fields. These representations, however, are beyond the scope of this paper.



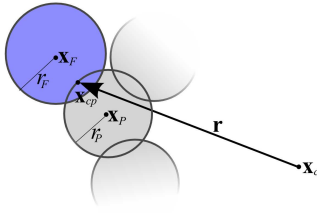


Fig. 3. Rigid particle  $\mathbf{x}_P$  and fluid particle  $\mathbf{x}_F$  in contact. The position  $\mathbf{x}_{cp}$  denotes the contact point of the fluid and the rigid body. The values  $r_F$  and  $r_P$  denote the radii of the respective particles. The vector  $\mathbf{r}$  denotes the distance of the contact point  $\mathbf{x}_{cp}$  to the center of mass  $\mathbf{x}_c$  of the rigid body.

## V. BOUNDARY HANDLING

In this section, we introduce a novel technique to enforce boundary conditions for particle-based rigid-fluid contacts. Boundary conditions model the relative velocities and positions of the fluid at the boundary. Our approach allows to control both the normal and tangential relative velocities and the relative positions effectively to realize various boundary conditions. The relative velocities and positions are controlled in separate substeps as e.g. proposed in [4], [53] for collision and contact handling of rigid and deformable solids. The boundary model for the relative velocities is discussed in Sec. V-A. Enforcing the desired velocities and positions is realized using a direct forcing approach discussed in Sec. V-B and V-C, respectively. It is implemented in a predictor-corrector fashion. Non-penetration is thereby addressed. In Sec. V-D, we discuss the entire pipeline of a single simulation step. At the end, simplifications for one-way solid-to-fluid coupling and static boundaries are discussed. To detect collisions, we follow [53] in advancing the positions without boundary forces and performing the collision detection on that advanced positions. Intermediate advanced values are denoted with a single or double asterisk (\*, \*\*).

### A. Controlling the relative velocity

In this section, we discuss the employed model for the velocity control at the boundary. As noted in Sec. IV, rigid bodies are sampled with particles. If we detect a collision between a fluid particle with position  $\mathbf{x}_F$ , velocity  $\mathbf{v}_F$ , mass  $m$  and a rigid body particle  $\mathbf{x}_P$ , we calculate a contact point  $\mathbf{x}_{cp} = \mathbf{x}_P + r_P \mathbf{n}$  at the boundary of the colliding rigid body particle (see Fig. 3).  $\mathbf{n}$  denotes the unit surface normal of the rigid body at  $\mathbf{x}_{cp}$ .  $m_c$  is the total mass of the colliding rigid body.

The rigid body velocity at the contact point is given by

$$\mathbf{v}_{cp}^*(t+h) = \mathbf{v}_c^*(t+h) + \omega_c^*(t+h) \times \mathbf{r}^*(t+h) \quad (7)$$

with  $\mathbf{r}^*(t+h) = \mathbf{x}_{cp}^*(t+h) - \mathbf{x}_c^*(t+h)$  being the relative position of  $\mathbf{x}_{cp}^*(t+h)$  with respect to the center of mass  $\mathbf{x}_c^*(t+h)$  of the rigid body.  $\mathbf{v}_c^*(t+h)$  and  $\omega_c^*(t+h)$  denote the linear and angular velocity of the rigid body, respectively.

Now, we want to impose a boundary condition on the relative velocity  $\mathbf{v}_r = \mathbf{v}_F - \mathbf{v}_{cp}$  of the following form:

$$\mathbf{v}_r(t+h) := \mathbf{v}_F(t+h) - \mathbf{v}_{cp}(t+h) = \varepsilon [\mathbf{v}_r^*(t+h)]_t - \delta [\mathbf{v}_r(t)]_n. \quad (8)$$

The current normal velocity is thereby given as  $[\mathbf{v}_r(t)]_n = (\mathbf{v}_r(t) \cdot \mathbf{n})\mathbf{n}$  and the uncontrolled tangential velocity of the next time step is given as  $[\mathbf{v}_r^*(t+h)]_t = \mathbf{v}_r^*(t+h) - [\mathbf{v}_r^*(t+h)]_n$ . The first term of (8) controls the slip. It can be used to damp the relative

tangential velocity of the fluid and the rigid body. Here, we use the predicted velocity of the subsequent timestep to properly consider accelerations due to body forces such as gravity. E.g., for a free-slip condition, the component of the fluid velocity tangential to a vertical boundary would not be damped. The second term of (8) controls the elasticity of the collision.  $\delta$  is called the coefficient of restitution.  $\delta = 1.0$  thereby corresponds to a perfectly elastic collision, while  $\delta = 0.0$  results in a perfectly inelastic collision. If not stated otherwise, we use  $\delta = 0.0$  in our scenarios, i.e. the relative normal velocity between the fluid and the rigid body at the boundary layer is zero. Both damping parameters  $\varepsilon$  and  $\delta$  are always in the interval  $[0, 1]$ .

To avoid sticking, we substitute the boundary condition (8) by

$$\mathbf{v}_r(t+h) = \varepsilon [\mathbf{v}_r^*(t+h)]_t + [\mathbf{v}_r^*(t+h)]_n \quad (9)$$

for  $\mathbf{v}_r^*(t+h) \cdot \mathbf{n} > 0$ . This leaves the normal component of the relative velocity unchanged if the fluid particle and the rigid body are moving away from each other. To simplify the subsequent explanations, we generally use (8) and omit (9) due to the similarities of both cases.

### B. Velocity update

In this section, the enforcement of the velocity constraints is described. We first handle the case of a single fluid particle in contact with a rigid body. Then, we generalize the idea to several fluid particles in contact with a single rigid body. For a single fluid particle with index  $i$ , the contact point of the fluid particle with the rigid body has the absolute position  $\mathbf{x}_{cp,i}^*(t+h)$  and the relative position  $\mathbf{r}_i^*(t+h)$  with respect to the center of mass of the rigid body. To enforce our boundary condition (8) on the relative velocity  $\mathbf{v}_{r,i}$ , we exchange a control force  $\mathbf{F}_i$  between the fluid particle and the rigid body. Assuming a simple Euler step, we end up with the constrained velocities for the fluid particle

$$\mathbf{v}_i(t+h) = \mathbf{v}_i^*(t+h) + \frac{h}{m_i} \mathbf{F}_i \quad (10)$$

and the rigid body at the contact point

$$\begin{aligned} \mathbf{v}_{cp,i}(t+h) = & \mathbf{v}_{cp,i}^*(t+h) - \frac{h}{m_c} \mathbf{F}_i \\ & + h \tilde{\mathbf{r}}_i^*(t+h) \mathbf{I}^{-1}(t) \tilde{\mathbf{r}}_i^*(t+h) \mathbf{F}_i \end{aligned} \quad (11)$$

with  $\tilde{\mathbf{r}}$  being the cross product matrix of the vector  $\mathbf{r}$ . In order to predict the velocities  $\mathbf{v}_i^*(t+h)$  and  $\mathbf{v}_{cp}^*(t+h)$ , we take into account all forces such as pressure forces, viscous forces and gravity.

Using the right hand sides of (10) and (11) for the relative velocity  $\mathbf{v}_{r,i}(t+h)$  in the constraint equation (8) and solving for the unknown control force  $\mathbf{F}_i$  yields

$$\mathbf{F}_i = \frac{1}{h} \left[ \left( \frac{1}{m_i} + \frac{1}{m_c} \right) \mathbf{E}_3 + \tilde{\mathbf{r}}_i^{*T}(t+h) \mathbf{I}^{-1}(t) \tilde{\mathbf{r}}_i^*(t+h) \right]^{-1} \hat{\mathbf{v}}_i \quad (12)$$

with  $\hat{\mathbf{v}}_i := \varepsilon [\mathbf{v}_{r,i}^*(t+h)]_t - \delta [\mathbf{v}_{r,i}(t)]_n - \mathbf{v}_{r,i}(t+h)$  and the 3x3 identity matrix  $\mathbf{E}_3$ . If we have  $k$  fluid particles in contact with a single rigid body, solve each contact separately using (12), and simply add up the forces and torques on the rigid body, we term this **local approach**.

Now, we assume that a single rigid body is in contact with  $k$  fluid particles and we want to enforce all contact velocities simultaneously. This is termed **global approach**. Similar to the

case of a single contact, we apply symmetric control forces  $\mathbf{F}_i$  at each contact point. For the rigid body these control forces sum up to a net force  $\mathbf{F}$  and a net torque  $\tau$ :

$$\mathbf{F} = - \sum_i \mathbf{F}_i \quad (13)$$

$$\tau = - \sum_i \mathbf{r}_i^*(t+h) \times \mathbf{F}_i. \quad (14)$$

Once  $\mathbf{F}$  and  $\tau$  are known, we can calculate the future linear and angular velocity of the rigid body and thereby the rigid-body velocities  $\mathbf{v}_{cp,i}(t+h)$  at the  $i$ -th contact point. The velocities of the fluid particles  $\mathbf{v}_i(t+h)$  can then be calculated using the constraint equations

$$\mathbf{v}_i(t+h) = \varepsilon [\mathbf{v}_{r,i}^*(t+h)]_t - \delta [\mathbf{v}_{r,i}(t)]_n + \mathbf{v}_{cp,i}(t+h). \quad (15)$$

To derive our system of equations for  $\mathbf{F}$  and  $\tau$ , we express the future velocity at the  $i$ -th contact point as

$$\mathbf{v}_{cp,i}(t+h) = \mathbf{v}_{cp,i}^*(t+h) + \frac{h}{m_c} \mathbf{F} + h \tilde{\mathbf{r}}_i^{*T}(t+h) \mathbf{I}^{-1}(t) \tau. \quad (16)$$

Plugging this future velocity  $\mathbf{v}_{cp,i}(t+h)$  for the contact point and the future velocity  $\mathbf{v}_i(t+h) = \mathbf{v}_i^*(t+h) + \frac{h}{m_i} \mathbf{F}_i$  for the fluid particle into the constraint equation (15) and solving for the unknown constraint force  $\mathbf{F}_i$  yields

$$\mathbf{F}_i = \frac{m_i}{h} \left[ \hat{\mathbf{v}}_i + \frac{h}{m_c} \mathbf{F} + h \tilde{\mathbf{r}}_i^{*T}(t+h) \mathbf{I}^{-1}(t) \tau \right] \quad (17)$$

with the unknown net force  $\mathbf{F}$  and the net torque  $\tau$  on the right hand side. The control forces  $\mathbf{F}_i$  are now plugged into the equations (13) and (14) for the net force  $\mathbf{F}$  and torque  $\tau$  on the rigid body. As a result, we get the symmetric, positive definite 6x6 linear system of equations for the unknowns  $\mathbf{F}$  and  $\tau$

$$\mathbf{A} \begin{bmatrix} \frac{1}{m_c} \mathbf{F} \\ \mathbf{I}^{-1}(t) \tau \end{bmatrix} = \begin{bmatrix} - \sum \frac{m_i}{h} \hat{\mathbf{v}}_i \\ - \sum \frac{m_i}{h} \tilde{\mathbf{r}}_i^{*T}(t+h) \hat{\mathbf{v}}_i \end{bmatrix} \quad (18)$$

with the system matrix

$$\mathbf{A} := \begin{bmatrix} (m_c + \sum m_i) \mathbf{E}_3 & \sum m_i \tilde{\mathbf{r}}_i^{*T}(t+h) \\ \sum m_i \tilde{\mathbf{r}}_i^{*T}(t+h) & \mathbf{I}(t) + \sum m_i \tilde{\mathbf{r}}_i^{*T}(t+h) \tilde{\mathbf{r}}_i^{*T}(t+h) \end{bmatrix}.$$

The employed concept is closely related to the interpenetration resolution scheme of [4], [5]. In this approach, collisions between several rigid bodies are handled by setting one rigid body as central body and the others as outer bodies. The outer bodies are pushed out of the central body in a two-way coupled fashion. However, instead of interpenetration resolution we adopt this method to enforce our boundary velocity constraints in a two-way coupled fashion by applying symmetric forces.

Since the velocities of the fluid particles at the boundary are completely determined by the constraint equations, the boundary velocity calculations for  $k$  contact points at a single rigid body can be reduced to the linear 6x6 system of equations in (18). In Sec. VI, we discuss several experiments using both the local and the global approach. Additionally, we compare the performance of both approaches.

This section has discussed the velocity update of the rigid body and the fluid particles. The position update for interpenetration handling is addressed in the following section.

### C. Position update

In addition to the correct relative velocity at the boundary, we want to enforce non-penetration of the fluid particles with respect to the boundary. We therefore control the position of the fluid particles at the boundary in a separate substep. We enforce the centers of the boundary fluid particles with radius  $r_i$  to retain a distance  $r_i$  to the contact point  $\mathbf{x}_{cp,i}$ . Since we have considered this contact point for the computation of the control force, such a position correction does not influence the slip condition. The corrected position update is implemented using an additional control impulse  $\mathbf{j}_i = j_i \mathbf{n}$  acting in normal direction, that is only applied in the position update of the integration step. It is calculated in the same manner as the control force for the velocity update. To meet the desired distance, we need to enforce

$$[\mathbf{x}_i^{**}(t+h) + h \mathbf{j}_i - \mathbf{x}_{cp,i}(t+h)] \cdot \mathbf{n} = r_F. \quad (19)$$

As the update is only applied to the fluid particles, we can use the final contact point position  $\mathbf{x}_{cp,i}(t+h)$ . Both,  $\mathbf{x}_{cp,i}(t+h)$  and the predicted future fluid positions  $\mathbf{x}_i^{**}(t+h)$  are calculated using the modified velocities from the subsequent step. The control impulses  $\mathbf{j}_i$  are then computed as

$$\mathbf{j}_i = \frac{1}{h} [(\mathbf{x}_{cp,i}(t+h) - \mathbf{x}_i^{**}(t+h)) \cdot \mathbf{n} + r_F] \mathbf{n}. \quad (20)$$

Unfortunately, the position update leads to a higher compression of the fluid at the boundary layer. However, higher density ratios are rapidly balanced in subsequent timesteps with the employed weakly compressible pressure approach. The maximum density ratios encountered in our simulations are given in Table I.

### D. Two-way coupling

In Alg. 1, we show all stages of a single simulation step. As we need to know the unconstrained velocities  $\mathbf{v}_i^*(t+h)$  and  $\mathbf{v}_{cp,i}^*(t+h)$  to calculate our control force  $\mathbf{F}$  and torque  $\tau$ , we perform a predictive integration step for the fluid and the rigid bodies. In the correction step, we only consider fluid particles and rigid bodies that are in contact. The same holds for the position update. We thereby take into account the modified velocities. Overall, up to three collision detection steps are performed.

---

**Algorithm 1** Pseudo code for two-way coupled moving boundaries

---

**Require:**  $n$  fluid particles,  $m$  rigid bodies

- 1: Detect fluid-fluid collisions
  - 2: Calculate fluid and rigid-body forces
  - 3: Integrate fluid and rigid body (prediction)  $\mathbf{x}(t) \rightarrow \mathbf{x}^*(t+h)$ ,  
 $\mathbf{v}(t) \rightarrow \mathbf{v}^*(t+h)$
  - 4: Detect rigid-fluid collisions
  - 5: Calculate net force  $\mathbf{F}$  and net torque  $\tau$
  - 6: Integrate fluid and rigid body (correction)  $\mathbf{x}^*(t) \rightarrow \mathbf{x}^{**}(t+h)$ ,  
 $\mathbf{v}^*(t+h) \rightarrow \mathbf{v}(t+h)$
  - 7: **if** (any contacts in 4) **then**
  - 8: Detect rigid-fluid collisions
  - 9: Correct fluid positions  $\mathbf{x}^{**}(t+h) \rightarrow \mathbf{x}(t+h)$
  - 10: **end if**
- 

Steps 7-9 in Alg. 1 are only performed once, even if some penetrations are not resolved due to conflicting constraints. See Sec. VII for some notes on this issue.

### E. One-way solid-to-fluid coupling and static boundaries

For the two-way coupling, we need up to three collision detection steps which are comparatively time-consuming. In some cases, however, the influence of the fluid on the solid is small and could be neglected (e.g. heavy objects) or the solid does not move at all. For this case, we propose to use a more efficient one-way solid-to-fluid coupling. In this one-way coupling, the solid influences the fluid, but not vice versa. The rigid body velocity at the contact point in (11) or (16), respectively, thereby simplifies to

$$\mathbf{v}_{cp,i}(t+h) = \mathbf{v}_{cp,i}^*(t+h) \quad (21)$$

for one-way coupling or

$$\mathbf{v}_{cp,i}(t+h) = \mathbf{v}_{cp,i}(t) = 0 \quad (22)$$

for static boundaries, respectively. The fluid velocity can be calculated from the boundary conditions (8) in the usual way.

As the rigid body is integrated prior to the control force calculation and as the rigid body is not affected by any corrections, we can calculate the velocity and position correction for the fluid in one step. This saves one collision detection step compared to the two-way coupling. As the collision detection is comparatively time-consuming, the efficiency can be significantly improved using the one-way coupling. Additionally, there is no need to solve a system of equations, as the fluid velocities can be directly computed from the boundary conditions. All stages of a single simulation step for the one-way coupling are summarized in Alg. 2.

---

#### Algorithm 2 Pseudo code for one-way coupled boundaries

---

**Require:**  $n$  fluid particles,  $m$  rigid bodies

- 1: Detect fluid-fluid collisions
  - 2: Calculate fluid and rigid body forces
  - 3: Integrate fluid and rigid body (prediction)  $\mathbf{x}(t) \rightarrow \mathbf{x}^*(t+h)$ ,  
 $\mathbf{v}(t) \rightarrow \mathbf{v}^*(t+h)$
  - 4: Detect fluid-rigid collisions
  - 5: Calculate fluid velocity and position (correction)  $\mathbf{x}^*(t+h) \rightarrow$   
 $\mathbf{x}(t+h)$ ,  $\mathbf{v}^*(t+h) \rightarrow \mathbf{v}(t+h)$
- 

### F. Parameters

The timestep for the simulation is chosen according to the Courant-Friedrichs-Lewy (CFL) convergence condition. The resulting timestep is generally rather restrictive with respect to stability of the fluid and it has turned out that the simulations remain stable when the two- or one-way coupling is incorporated. For the rigid-fluid interaction, we basically need to ensure that two particles do not move more than their diameter towards each other in one timestep. In the experiments, we use timesteps ranging from  $6 \cdot 10^{-5}$  to  $1.5 \cdot 10^{-4}$ .

The estimation of appropriate parameters for different boundary conditions can be a tedious task, particularly as the effects of the parameters typically depend on the timestep. In our approach, the handling of parameters is comparatively easy. First of all, the total number of free parameters is only two, namely the damping parameters  $\varepsilon, \delta$ . Second,  $\varepsilon, \delta$  are always in the interval  $[0, 1]$ .

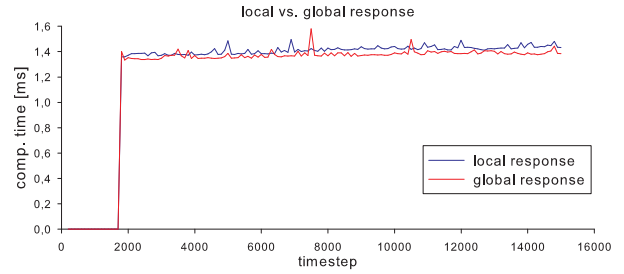


Fig. 4. The diagram shows the computation time for the local and the global response scheme for the sinking ship scene. Both are linear in the number of contacts and make up only a small fraction of the total computation time of 250-280ms.

### G. Implementation issues

The efficient detection of particle-particle contacts is one of the fundamental issues in particle-based fluid simulations. Similar to [57], we use a uniform spatial subdivision and store the results in a hash table [58]. We also follow [57] in employing temporal coherence, i.e. we only update the information of particles if their grid cell has changed. Due to the restrictive timestep, temporal coherence significantly speeds up the insertion of particles into the hash table.

## VI. RESULTS

In this section, we illustrate the capabilities of our boundary handling technique with 2D and 3D experiments that range from some simple explanatory scenes to high-velocity impacts. We make use of both the local and the global approach for updating the boundary velocity. The following experiments are performed: As many authors use penalty methods in their simulations, we first compare the proposed approach to the penalty approach of [2]. Then, we demonstrate different slip conditions in a 2D setting. Handling high-velocity impacts and one-way coupling is illustrated with a stone impacting a water basin. Sec. VI-E and VI-F illustrate buoyancy and drag effects. Finally, we show some advanced two-way coupled scenes.

Tab. I gives an overview of the performance for the scenarios. All performance measurements are given with respect to an Intel Dual Core 2.13 GHz with 4 GB of RAM, running a single-threaded version of the simulation. In all simulations, we use an explicit leapfrog integration scheme. If not stated otherwise, the viscosity is set to  $\nu = 0.1$ . As pointed out in [8], the compressibility of the fluid is governed by the speed of sound. The speed of sound has been chosen with respect to the maximum relative velocity between fluid and solids to ensure a certain density ratio. Both values, the speed of sound and the measured density ratio are stated in Tab. I. We also give the performance for a single fluid calculation step without boundary handling and a complete simulation step including the boundary handling.

For the performed experiments, we have used either the local or the global approach. Both approaches are linear in the number of contacts and make up less than 1% of the total computation time in most scenarios. Both approaches show plausible results, whereas in the global approach the boundary velocities are met more accurately. All timings in Tab. I are given using the local approach. In Fig. 4, we compare the local and the global response with respect to their performance for the sinking ship scene illustrated in Fig. 5.



TABLE I

SOME EXEMPLARY SCENES: NUMBER OF PARTICLES, COMPUTATION TIME FOR ONE SIMULATION STEP, SOUND SPEED AND MAXIMUM DENSITY RATIO.

scene	fluid particles	cluster particles	fluid calc. [s]	simulation step [s]	speed of sound	max density ratio
Impact	850k	9k	3.47	7.07	600	1.19
Floating cuboids	2M	7.5k	5.79	11.4	250	1.13
Floating spheres	130k	760	0.56	1.14	250	1.026
Stone-skipping	240k	94	0.83	1.64	300	1.07
Flotsam	2.57M	18.6k	7.61	15.03	225	1.16

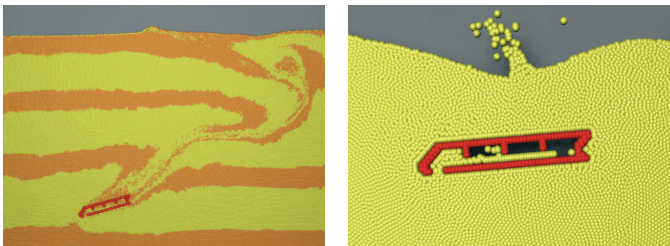


Fig. 5. Two-way coupling of a sinking ship with a fluid. Colored particles on the left indicate the flow of the fluid. The picture on the right indicates the accuracy of the boundary handling.

For the reconstruction of the fluid surface, we employ marching cubes [59], while single particles are handled as blobs. Triangulated surfaces are employed for visualizing the rigid bodies. Surfaces and blobs are rendered in POV-Ray (<http://www.povray.org>). In some cases, we visualize the underlying particle simulation for illustration purposes.

#### A. Comparison to a penalty based approach

Many authors employ penalty methods for handling boundaries in particle-based simulations. We compare the proposed local approach with the penalty based approach of [2]. We have chosen a 2D example of a leaking ship sinking into a fluid to illustrate the effects of both boundary methods without getting distracted by the surface reconstruction. Large parts of the ship are only represented by a single layer of particles. As for the penalty method, several effects can be observed in the experiment:

- Penalty methods offer only limited control. To ensure non-penetration, large penalty forces have to be applied. This leads to elastic collisions with an unknown coefficient of restitution.
- Penalty methods can only react in a subsequent timestep, if a penetration has already occurred. Therefore, the distance of fluid particles to the boundary slightly varies over time. Additionally, unnatural accelerations can occur. For the sinking ship, this leads to the effect that the ship is not correctly filled and single particles are bouncing on the surface.

The proposed local and the global approach can cope with these issues. As velocity and position are controlled in different sub-steps, non-penetration and inelastic collision can be realized at the same time. As velocity and position are predicted and corrected in the same simulation step, constant distances can be realized and unnatural accelerations of fluid particles at the boundary are avoided. The ship is properly filled with fluid particles and sinks into the basin. Even in case where it is fully submerged, non-penetration with constant distance can be enforced. Some results can be seen in Fig. 5.

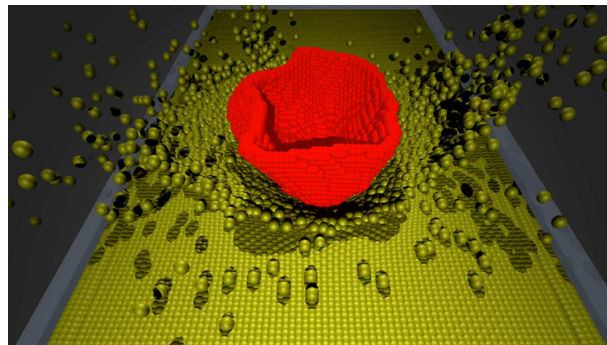


Fig. 6. A vessel is floating in a water basin. No fluid is leaking through the boundary.

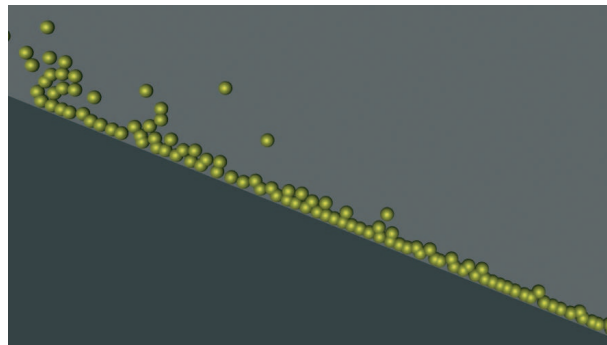


Fig. 7. Experimental set-up for the slip condition.

#### B. Accuracy

To illustrate accuracy and non-penetration of our method in 3D, we simulate a vessel falling into a large basin of fluid. Fig. 6 illustrates this setting. Although the boundary is represented only by a single layer of particles, no fluid is leaking through the boundary. The velocity update is performed using the local approach.

#### C. Slip condition

Imposing different kinds of slip conditions is a challenging issue. However, using the proposed method, slip can easily be controlled. In Fig. 7, we show the experimental setup for the illustration of different slip conditions. Particles are emitted on the left-hand side, flowing down a static ramp. Different slip condition ranging from  $\varepsilon = 0.0$  (no-slip) to  $\varepsilon = 1.0$  (free-slip) lead to different flow properties. We refer the reader to the accompanying video to assess the effects in a dynamic simulation.

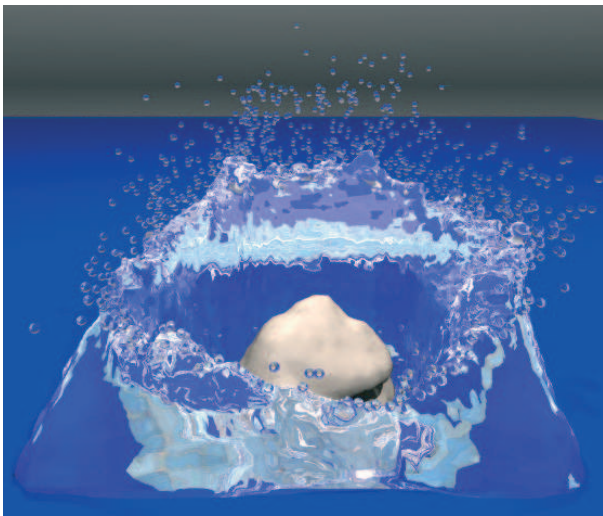


Fig. 8. Impact: High-velocity impact of an asteroid.

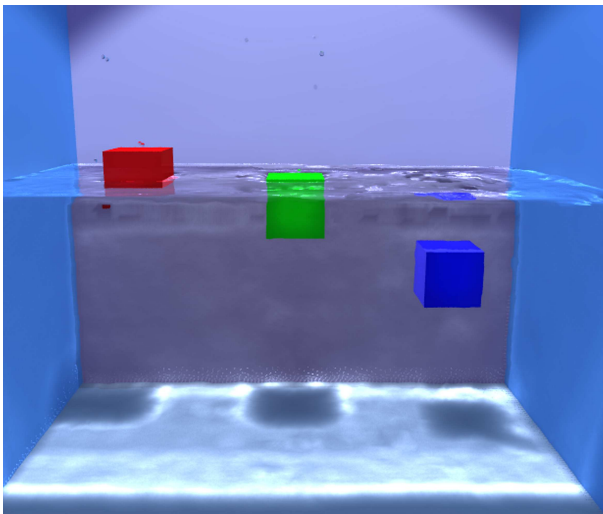


Fig. 9. Buoyancy effects: Cuboids of different densities dropped into a fluid.

#### D. One-way solid-to-fluid coupling

Fig. 8 illustrates one-way solid-to-fluid coupling with an impact scene of an asteroid model. Due to the high velocity of the asteroid, the speed of sound is set to 600. The maximum density ratio at the time of the impact is 1.19. For the rest of the simulation, the density ratio is below 1.1. The experiment indicates that high relative velocities can be handled.

#### E. Buoyancy effects

In Fig. 9, we illustrate that buoyancy effects are properly captured using the proposed global response scheme. Three cuboids of different densities are dropped into a fluid. As expected, the lightest cube (red) is floating, the cube with medium density (green) is sinking slowly and the heaviest cube (blue) is sinking fast.

#### F. Drag effects

Some approaches such as [46] take into account only the pressure forces acting on the boundary. Effects due to dynamics forces such as viscosity, are not properly captured. The following

experiment illustrates that the influence of dynamic forces on moving rigid bodies is properly captured with our method. A rigid sphere is dropped into fluids of different viscosities ( $\nu = 0.1$ ,  $\nu = 3.0$ ). Fig. 10 depicts both scenarios at the same time point. The images show that the sphere is sinking deeper in the low-viscous fluid compared to the high-viscosity fluid. The local velocity update is employed for the boundary handling in this setting.

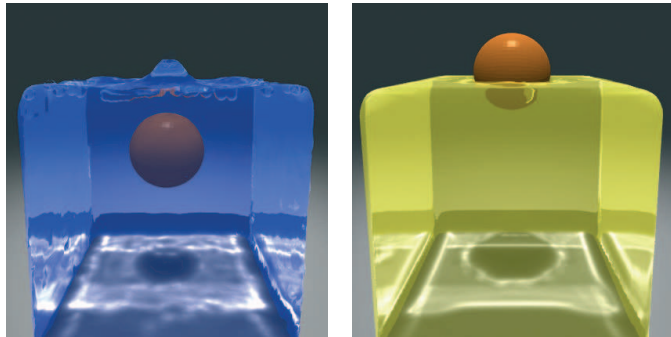


Fig. 10. Viscous effects: Spheres dropped into fluids with different viscosities. Viscosity is set to 0.1 in the left image and to 3.0 in the right image.

#### G. Two-way coupling

The following two experiments further illustrate the proposed two-way coupling approach. Fig. 1 and Fig. 11 show a stone-skipping experiment. Due to its high velocity, the stone is reflected at the fluid surface. The initial velocity is about 90% of the velocity of the impact scenario. For low velocities at the end, the stone finally sinks. Again, we would like to refer the reader to the accompanying video to assess the dynamics. In this scenario the local and the global boundary handling approach show very similar dynamics. Fig. 11 is simulated using the global approach. Fig. 1 illustrates the local approach.

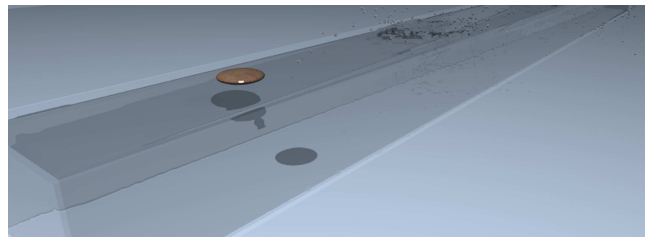


Fig. 11. Stone-skipping.

A second experiment to illustrate the two-way coupling is shown in Fig. 12. Here, complex-shaped rigid objects are floating on a wave. Again, the boundary handling is performed using the local approach.

## VII. CONCLUSION AND FUTURE WORK

We have presented an efficient Lagrangian method for the handling of fixed and moving boundaries. Direct forcing is employed to realize a large range of slip and Neumann boundary conditions. The proposed technique can be used for one- and two-way coupling with arbitrarily shaped boundaries that are represented with particles. Static and dynamic forces are properly taken into account to allow for buoyancy and drag effects. In





Fig. 12. Boundary handling for arbitrarily shaped objects illustrated with flotsam on the beach.

contrast to previous Lagrangian methods, overlaps of fluid and rigid-body particles are avoided. The proposed method is superior to previously used penalty-based approaches such as [2]. It offers a greater amount of control, ensures non-penetration and it does not introduce stiffness to the system. At the same time, it is computationally efficient and scales linearly in the number of contact points. We have made several tests using two variants of the approach, namely handling each contact point separately and solving all boundary velocities at once. Both methods show plausible results and a very similar performance. While the global approach is more accurate, the local approach allows to directly process collision pairs. The set up of a system of equations is thereby avoided.

The presented schemes work with compressible and weakly compressible models. This restriction allows to avoid global computations, i.e. computations that take into account the state of the whole fluid domain. Since particle-based fluids scale well for large scenes, the proposed boundary handling approach is particularly interesting for complex scenes with irregular simulation domains. Further, the underlying model for controlling the relative velocities is easy to adjust, as the number of free parameters is low. Additionally, the range of the parameters is known.

We currently do not handle simultaneous contact of a single fluid particle with more than one rigid body and simultaneous contact of several rigid bodies in a fluid. We believe that sophisticated but often expensive methods such as contact graphs could be employed to handle such settings.

## VIII. ACKNOWLEDGMENTS

The digital asteroid model of the impact scene is courtesy of Scott Hudson, Washington State University. The bunny model is courtesy of the Computer Graphics Laboratory at Stanford University. We would like to thank the reviewers for their valuable suggestions during the review process that helped to improve the global approach.

## REFERENCES

[1] R. Bridson and M. Müller-Fischer, “Fluid simulation: SIGGRAPH 2007 Course Notes,” in *SIGGRAPH '07: ACM SIGGRAPH 2007 courses*. New York, NY, USA: ACM Press, 2007, pp. 1–81.

[2] J. Monaghan, “Smoothed Particle Hydrodynamics,” *Reports on Progress in Physics*, vol. 68, no. 8, pp. 1703–1759, 2005.

[3] S. Hieber, “Particle-methods for flow-structure interactions,” Ph.D. dissertation, Swiss Federal Institute of Technology Zürich (ETHZ), 2007.

[4] T. Shinar, C. Schroeder, and R. Fedkiw, “Two-way coupling of rigid and deformable bodies,” in *ACM SIGGRAPH/Eurographics Symposium on Computer Animation (SCA)*, 2008.

[5] T. Shinar, “Simulation of coupled rigid and deformable solids and multiphase fluids,” Ph.D. dissertation, Stanford University, June 2008.

[6] J. Bonet and S. Kulasegaram, “A simplified approach to enhance the performance of smooth particle hydrodynamics methods,” *Applied Mathematics and Computation*, vol. 126, no. 2-3, pp. 133–155, 2002.

[7] J. Monaghan, “Simulating Free Surface Flows with SPH,” *Journal of Computational Physics*, vol. 110, no. 2, pp. 399–406, 1994.

[8] M. Becker and M. Teschner, “Weakly Compressible SPH for Free Surface Flows,” in *Proc. of ACM SIGGRAPH/Eurographics Symposium on Computer Animation*, August 2007, pp. 63–72.

[9] J. Chen and N. Lobo, “Toward Interactive-Rate Simulation of Fluids with Moving Obstacles Using Navier-Stokes Equations,” *Graphical Models and Image Processing*, vol. 57, no. 2, pp. 107–116, 1995.

[10] N. Foster and D. Metaxas, “Realistic Animation of Liquids,” *Graphical Models and Image Processing*, vol. 58, no. 5, pp. 471–483, 1996.

[11] N. Foster and D. Metaxas, “Controlling fluid animation,” *Computer Graphics International*, vol. 97, pp. 178–188, 1997.

[12] J. Stam, “Stable Fluids,” *Proceedings of the 26th annual conference on Computer graphics and interactive techniques*, pp. 121–128, 1999.

[13] R. Fedkiw, J. Stam, and H. W. Jensen, “Visual simulation of smoke,” in *SIGGRAPH '01: Proceedings of the 28th annual conference on Computer graphics and interactive techniques*. New York, NY, USA: ACM, 2001, pp. 15–22.

[14] N. Foster and R. Fedkiw, “Practical animation of liquids,” in *SIGGRAPH '01: Proceedings of the 28th annual conference on Computer graphics and interactive techniques*. New York, NY, USA: ACM Press, 2001, pp. 23–30.

[15] T. Takahashi, H. Fujii, A. Kunimatsu, K. Hiwada, T. Saito, K. Tanaka, and H. Ueki, “Realistic Animation of Fluid with Splash and Foam,” *Computer Graphics Forum*, vol. 22, no. 3, pp. 391–400, 2003.

[16] G. D. Yngve, J. F. O’Brien, and J. K. Hodgins, “Animating Explosions,” in *SIGGRAPH '00: Proceedings of the 27th annual conference on Computer graphics and interactive techniques*. New York, NY, USA: ACM Press/Addison-Wesley Publishing Co., 2000, pp. 29–36.

[17] F. Losasso, F. Gibou, and R. Fedkiw, “Simulating Water and Smoke with an Octree Data Structure,” in *SIGGRAPH '04: ACM SIGGRAPH 2004 Papers*. New York, NY, USA: ACM, 2004, pp. 457–462.

[18] G. Irving, E. Guendelman, F. Losasso, and R. Fedkiw, “Efficient simulation of large bodies of water by coupling two and three dimensional techniques,” in *SIGGRAPH '06: ACM SIGGRAPH 2006 Papers*. New York, NY, USA: ACM, 2006, pp. 805–811.

[19] B. M. Klingner, B. E. Feldman, N. Chentanez, and J. F. O’Brien, “Fluid animation with dynamic meshes,” *ACM Trans. Graph.*, vol. 25, no. 3, pp. 820–825, 2006.

[20] N. Chentanez, B. E. Feldman, F. Labelle, J. F. O’Brien, and J. R. Shewchuk, “Liquid Simulation on Lattice-Based Tetrahedral Meshes,” in *SCA '07: Proceedings of the 2007 ACM SIGGRAPH/Eurographics symposium on Computer animation*. Aire-la-Ville, Switzerland, Switzerland: Eurographics Association, 2007, pp. 219–228.

[21] N. Chentanez, T. G. Goktekin, B. E. Feldman, and J. F. O’Brien, “Simultaneous Coupling of Fluids and Deformable Bodies,” in *SCA '06: Proceedings of the 2006 ACM SIGGRAPH/Eurographics symposium on Computer animation*. Aire-la-Ville, Switzerland, Switzerland: Eurographics Association, 2006, pp. 83–89.

[22] B. E. Feldman, J. F. O’Brien, B. M. Klingner, and T. G. Goktekin, “Fluids in deforming meshes,” in *SCA '05: Proceedings of the 2005 ACM SIGGRAPH/Eurographics symposium on Computer animation*. New York, NY, USA: ACM Press, 2005, pp. 255–259.

[23] C. Batty, F. Bertails, and R. Bridson, “A Fast Variational Framework for Accurate Solid-Fluid Coupling,” in *SIGGRAPH '07: ACM SIGGRAPH 2007 papers*. New York, NY, USA: ACM Press, 2007, p. 100.

[24] Y. Zhu and R. Bridson, “Animating Sand as a Fluid,” in *SIGGRAPH '05: ACM SIGGRAPH 2005 Papers*. New York, NY, USA: ACM Press, 2005, pp. 965–972.

[25] M. Carlson, P. Mucha, and G. Turk, “Rigid Fluid: Animating the Interplay Between Rigid Bodies and Fluid,” in *SIGGRAPH '04: ACM SIGGRAPH 2004 Papers*. New York, NY, USA: ACM Press, 2004, pp. 377–384.

- [26] O. G enevaux, A. Habibi, and J. Dischler, "Simulating Fluid-Solid Interaction," *Graphics Interface Proceedings 2003: Canadian Human-Computer Communications Society*, 2003.
- [27] E. Guendelman, A. Selle, F. Losasso, and R. Fedkiw, "Coupling water and smoke to thin deformable and rigid shells," in *SIGGRAPH '05: ACM SIGGRAPH 2005 Papers*. New York, NY, USA: ACM Press, 2005, pp. 973–981.
- [28] Y. Liu, X. Liu, and E. Wu, "Real-Time 3D Fluid Simulation on GPU with Complex Obstacles," in *Proc. of 12th Pacific Conference on Computer Graphics and Applications*, 2004, pp. 247–256.
- [29] C. Peskin, "Flow Patterns around Heart Valves: A Numerical Study," *J. Comp. Phys.*, vol. 10, pp. 252–271, 1972.
- [30] C. Peskin, "The Immersed Boundary Method," *Acta Numerica*, vol. 11, pp. 479–517, 2002.
- [31] E. A. Fadlun, R. Verzicco, P. Orlandi, and J. Mohd-Yusof, "Combined Immersed-Boundary Finite-Difference Methods for Three-Dimensional Complex Flow Simulations," *Journal of Comp. Phys.*, vol. 161, no. 1, pp. 35–60, 2000.
- [32] M. Uhlmann, "An immersed boundary method with direct forcing for the simulation of particulate flows," *Journal of Computational Physics*, vol. 209, pp. 448–476, 2005.
- [33] J.-I. Choi, R. C. Oberoi, J. R. Edwards, and J. A. Rosati, "An immersed boundary method for complex incompressible flows," *J. Comput. Phys.*, vol. 224, no. 2, pp. 757–784, 2007.
- [34] D. Le, B. Khoo, and J. Peraire, "An immersed interface method for viscous incompressible flows involving rigid and flexible boundaries," *Journal of Computational Physics*, vol. 220, no. 1, pp. 109–138, 2006.
- [35] R. Fedkiw, "Coupling an Eulerian fluid calculation to a Lagrangian solid calculation with the ghost fluid method," *Journal of Computational Physics*, vol. 175, no. 1, pp. 200–224, 2002.
- [36] C. Hirt, A. Amsden, and J. Cook, "An arbitrary Lagrangian-Eulerian computing method for all flow speeds," *Journal of Computational Physics*, vol. 14, no. 3, pp. 227–253, 1974.
- [37] F. Losasso, J. Talton, N. Kwatra, and R. Fedkiw, "Two-way coupled SPH and Particle Level Set Fluid Simulation," *IEEE TVCG*, 2008, in press.
- [38] A. Robinson-Mosher, T. Shinar, J. Gretarsson, J. Su, and R. Fedkiw, "Two-way coupling of fluids to rigid and deformable solids and shells," *ACM Trans. on Graphics*, vol. 27, 2008, in press.
- [39] R. Keiser, B. Adams, D. Gasser, P. Bazzi, P. Dutr e, and M. Gross, "A unified lagrangian approach to solid-fluid animation," in *Proceedings of the Eurographics Symposium on Point-Based Graphics*, 2005, pp. 125–134.
- [40] B. Solenthaler, J. Schl afi, and R. Pajarola, "A Unified Particle Model for Fluid Solid Interactions: Research Articles," *Comput. Animat. Virtual Worlds*, vol. 18, no. 1, pp. 69–82, 2007.
- [41] R. Keiser, B. Adams, P. Dutr e, L. Guibas, and M. Pauly, "Multiresolution particle-based fluids," ETH Zurich, Tech. Rep., 2006.
- [42] S. Falappi and M. Gallati, "SPH Simulation of Water Waves Generated by Granular Landslides," in *Proc. of 32nd Congress of IAHR (International Association of Hydraulic Engineering & Research)*, 2007.
- [43] M. M uller, S. Schirm, M. Teschner, B. Heidelberger, and M. Gross, "Interaction of Fluids with Deformable Solids," *Computer Animation and Virtual Worlds*, vol. 15, no. 34, pp. 159–171, 2004.
- [44] X. Hu and N. Adams, "A multi-phase SPH method for macroscopic and mesoscopic flows," *Journal of Computational Physics*, vol. 213, no. 2, pp. 844–861, 2006.
- [45] J. Morris, P. Fox, and Y. Zhu, "Modeling Low Reynolds Number Incompressible Flows using SPH," *Journal of Computational Physics*, vol. 136, no. 1, pp. 214–226, 1997.
- [46] G. Oger, M. Doring, B. Alessandrini, and P. Ferrant, "Two-dimensional SPH Simulations of Wedge Water Entries," *Journal of Computational Physics*, vol. 213, no. 2, pp. 803–822, 2006.
- [47] R. Weinstein, J. Teran, and R. Fedkiw, "Dynamic Simulation of Articulated Rigid Bodies with Contact and Collision," *IEEE TVCG*, vol. 12, no. 3, pp. 365–374, 2006.
- [48] M. M uller, B. Heidelberger, M. Hennix, and J. Ratcliff, "Position Based Dynamics," *J. Vis. Commun.*, vol. 18, no. 2, pp. 109–118, 2007.
- [49] R. Weinstein, E. Guendelman, and R. Fedkiw, "Impulse-Based Control of Joints and Muscles," *IEEE TVCG*, vol. 14, no. 1, pp. 37–46, 2008.
- [50] M. Gissler, M. Becker, and M. Teschner, "Local constraint methods for deformable objects," in *Proc. of Virtual Reality Interactions and Physical Simulations (VriPhys)*, November 2006, pp. 25–32.
- [51] E. Sifakis, T. Shinar, G. Irving, and R. Fedkiw, "Hybrid Simulation of Deformable Solids," in *Proceedings of the 2007 ACM SIGGRAPH/Eurographics symposium on Computer animation*. Eurographics Association Aire-la-Ville, Switzerland, Switzerland, 2007, pp. 81–90.
- [52] N. Th urey, K. Iglberger, and U. R ude, "Free Surface Flows with Moving and Deforming Objects with LBM," in *Proc. of Vision, Modeling, Visualization VMV'06*, 2006, pp. 193–200.
- [53] E. Guendelman, R. Bridson, and R. Fedkiw, "Nonconvex rigid bodies with stacking," *ACM Trans. Graph.*, vol. 22, no. 3, pp. 871–878, 2003.
- [54] R. Gingold and J. Monaghan, "Smoothed Particle Hydrodynamics - Theory and Application to Non-Spherical Stars," *Mon. Not. R. Astron. Soc.*, vol. 181, pp. 375–389, 1977.
- [55] L. Lucy, "A numerical approach to the testing of the fission hypothesis," *Astronomical Journal*, vol. 82, no. 12, pp. 1013–1024, 1977.
- [56] B. Adams, M. Pauly, R. Keiser, and L. J. Guibas, "Adaptively Sampled Particle Fluids," in *SIGGRAPH '07: ACM SIGGRAPH 2007 papers*. New York, NY, USA: ACM Press, 2007, p. 48.
- [57] N. Bell, Y. Yu, and P. J. Mucha, "Particle-Based Simulation of Granular Materials," in *SCA '05: Proceedings of the 2005 ACM SIGGRAPH/Eurographics symposium on Computer animation*. New York, NY, USA: ACM Press, 2005, pp. 77–86.
- [58] M. Teschner, B. Heidelberger, M. M uller, D. Pomeranets, and M. Gross, "Optimized Spatial Hashing for Collision Detection of Deformable Objects," in *Proc. of Vision, Modeling, Visualization VMV'03*, 2003, pp. 47–54.
- [59] W. E. Lorensen and H. E. Cline, "Marching cubes: A High Resolution 3D Surface Construction Algorithm," in *SIGGRAPH '87: Proc. of the 14th annual conference on Computer graphics and interactive techniques*, 1987, pp. 163–169.



**Markus Becker** received his Diploma in Mathematics from the University of Kaiserslautern in 2005. He is currently pursuing his PhD as a member of the Computer Graphics group at the University of Freiburg. His research interests are fluid dynamics and deformable modeling.



**Hendrik Tendorf** is a graduate student at the University of Freiburg. His research interests are optimization techniques and shared-memory parallelization.



**Matthias Teschner** is Professor of Computer Science and head of the Computer Graphics group at the University of Freiburg. He received his Ph.D. in Electrical Engineering from the University of Erlangen-Nuremberg in 2000. From 2001 to 2004, he was Research Associate at Stanford University and at the ETH Zurich. His research interests comprise physical simulation, computer animation, computational geometry, collision handling, and real-time rendering with applications in entertainment technology and medical simulation. He has published about 60 research papers. He has served on program committees of major Computer Graphics conferences including Eurographics, IEEE Visualization, ACM SIGGRAPH / Eurographics Symposium on Computer Animation, and Computer Graphics International. He also participates in the review process of a number of major Computer Graphics journals.